

# Enhanced nonlinearity for filamentation in gold-nanoparticle-doped water

Shuai Yuan (袁帅)<sup>1</sup>, Lirong Wang (王莉荣)<sup>1</sup>, Fengjiang Liu (刘峰江)<sup>2</sup>,  
Fengquan Zhou (周锋全)<sup>1</sup>, Min Li (李敏)<sup>1</sup>, Hui Xu (徐晖)<sup>1</sup>, Yuan Nie (聂源)<sup>1</sup>,  
Junyi Nan (南君义)<sup>2</sup>, and Heping Zeng (曾和平)<sup>1,2,\*</sup>

<sup>1</sup>Shanghai Key Laboratory of Modern Optical System, Engineering Research Center of Optical Instrument and System, Ministry of Education, School of Optical-Electrical and Computer Engineering, University of Shanghai for Science and Technology, Shanghai 200093, China

<sup>2</sup>State Key Laboratory of Precision Spectroscopy, East China Normal University, Shanghai 200062, China

\*Corresponding author: hpzeng@phy.ecnu.edu.cn

Received October 17, 2018; accepted December 7, 2018; posted online February 27, 2019

We report a universal approach based on the surface plasmon resonances (SPRs) attained in filamentation in water doped with gold nanoparticles for enhancing the nonlinear refractive index. The filament-induced supercontinuum spectrum in water overlaps with SPRs of gold nanospheres, which further leads to a modification on the Kerr nonlinear refractive index. In our experiment, the measured nonlinear refractive index ( $n_2$ ) in water doped with gold nanoparticles increases by six times, as compared with that in pure water. Such enhancement may be useful for filament-induced nonlinear applications with modest incident intensity.

OCIS codes: 260.5950, 320.7110, 320.6629, 160.4236.

doi: 10.3788/COL201917.032601.

The drive to study filamentation-induced nonlinear optics in condensed media<sup>[1–16]</sup> is fueled by a host of tantalizing potential applications like spatial and spectral reshaping of pulses<sup>[4]</sup>, shock wave formation<sup>[17–19]</sup>, supercontinuum generation<sup>[20]</sup>, microbubbles creation<sup>[21–23]</sup>, and nanoparticles production<sup>[24]</sup>. Many of these applications are limited by weak nonlinearities, demanding high pumping thresholds. To enhance the nonlinear response of a material, one of the approaches consists of creating artificial electromagnetic resonances by stacking materials of different refractive indices or using other types of composite materials, since resonant nonlinearities can be several orders of magnitude stronger than nonresonant ones<sup>[25–27]</sup>. A typical example is that of metal. Surface plasmon resonances (SPRs) induced by doping the material with metal nanoparticles or employing metallic nanostructures are known to exhibit strong field localization on ultrafast timescales<sup>[28–31]</sup>.

In 2007 and 2009, Wang *et al.*<sup>[30]</sup> and Driben *et al.*<sup>[31]</sup> launched filaments in silver-nanoparticle-doped water. The results showed that the efficiency of frequency conversion in silver-nanoparticle-doped water was significantly higher than that in pure water. While recently, in Ref. [32], supercontinuum emissions generated in water doped with gold nanoparticles (nanorods, resonant peak at 861 nm) were investigated. The generated supercontinuum spectrum was broader if the SPRs overlapped the incident spectrum. Although in previous works the intense supercontinuum emissions were explained by SPR-induced excitation<sup>[30–32]</sup>, resonant nonlinearities for filamentation in metal-nanoparticle-doped liquids are still left to be quantitatively investigated. Besides, in previous investigations by overlapping the SPRs with the incident spectrum<sup>[16,32]</sup>,

although the nonlinear refractive index was increased, the fundamental pulse would be strongly absorbed, which limited the length of the filament.

In this Letter, we create laser filamentation in gold-nanoparticle-doped water (nanospheres, resonant peak at 520 nm). Here, the SPRs overlap the generated white light spectrum in water other than the incident spectrum. We demonstrate that the filament-induced white light from 510 to 540 nm in doped water excites the electrons of gold nanoparticles through SPRs. Hence, it promotes the nonlinear response in water without resonant absorption of the fundamental pulses. The resonant nonlinearity is estimated to be increased by  $\sim 6$  times, which can be confirmed by the onset shift of the multiple filaments.

The experiments were carried out by using a Ti:sapphire chirped pulse amplification laser system (60 fs, 1 kHz, 800 nm), which provided pulses of maximum energy up to 2.4 mJ. The setup is shown in Fig. 1. The power of the laser pulse was adjusted by a variable attenuator. A fused silica cuvette was 100 mm  $\times$  20 mm  $\times$  20 mm in size, 1.5 mm for the thickness of each side, and open on top. The filament was created by focusing the laser beam with a fused silica lens (F1,  $f = 21$  cm). It was located at  $\sim 50$  mm behind the fore wall of the cuvette when the cuvette was filled with gold-nanoparticle-doped water. A CCD camera (1280 pixel  $\times$  1024 pixel) was mounted on the top of the cuvette in order to project the plasma channels in an area of 100 mm  $\times$  80 mm. The exposure time of the CCD was set as 100 ms. After the filament, the generated supercontinuum emissions were collected by two fused silica lenses F2 ( $f = 20$  cm) and F3 ( $f = 8$  cm) to a fiber-coupled spectrometer (Ocean Optics HR4000CG). Appropriate neutral density (ND) filters were put in front

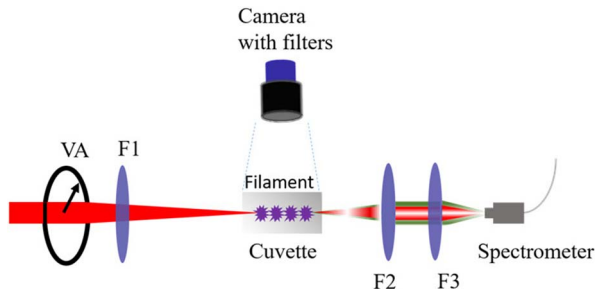


Fig. 1. Schematic diagram of the experimental setup. The laser pulses were focused by a fused silica lens F1 ( $f = 21$  cm) into pure water and doped water. Filament in the cuvette was imaged by a CCD camera with ND and bandpass filters in front. The output emission was collected and directed to a fiber-coupled spectrometer. VA, variable attenuator; CCD, charge-coupled device.

of the spectrometer in order to avoid CCD saturation. The doped water used here contained gold nanospheres in distilled water with  $\sim 12$  nm for the diameter and 250 ppm ( $1 \text{ ppm} = 10^{-6}$ ) for the concentration. Linear extinction spectra showed the resonant peak was centered at 520 nm. Here, the focal length of the external focusing (F1,  $f = 21$  cm) is our balanced choice, considering the plasma volume and the length of the filaments. In our experiment, with longer focal length ( $f > 30$  cm), the fluorescence of the filament in water cannot be clearly observed. While with tight focusing ( $f < 3$  cm), laser-induced breakdown dominates the propagation<sup>[7]</sup>.

During the experiment, we used two cuvettes of the same size. One was filled with distilled water. The other was filled with gold-nanoparticle-doped water. First, the filaments were investigated in distilled water under different input pulse energy. We took the top views and the output spectra of the filaments. Afterwards, the same measurements were repeated in doped water.

Figures 2(a), 2(c), and 2(e) show the top views of filaments generated in doped water and pure water. A band-pass filter (340–680 nm for the transmission band) was implemented in front of the CCD camera in order to

eliminate the scattered fundamental-wave components. The generated white light was scattered along the filament. In our experiment, the ranges of the longitudinal distribution of filament-induced supercontinuum in doped water were measured to be 11.8 and 15.6 mm under input pulse energy of 5.49 and 9.86  $\mu\text{J}$ , respectively [see Figs. 2(b), 2(d)], while in pure water the range was measured to be 700  $\mu\text{m}$  under input pulse energy of 9.72  $\mu\text{J}$  [see Fig. 2(f)]. Here, the filament in doped water was highly extended.

In Fig. 2, the onset of the filament starts closer to the focusing lens for higher input energy. Besides, under similar input pulse energy, the onset of the filament initiates even closer in doped water than in pure water. In the case of the external focusing, the focal position will be shifted due to self-focusing. The shift obeys the lens transformation formula,  $f' = \frac{f \cdot z_{\text{sf}}}{f + z_{\text{sf}}}$ .  $f'$  is the focal position under the circumstance with both geometrical focusing and self-focusing,  $f$  denotes the focal length of the external focusing lens, and  $z_{\text{sf}}$  represents the self-focusing distance of the parallel Gaussian beam given by Eq. (1)<sup>[33,34]</sup>;

$$z_{\text{sf}} = \frac{0.367ka^2}{\left\{ \left[ \left( \frac{P}{P_{\text{cr}}} \right)^{1/2} - 0.852 \right]^2 - 0.0219 \right\}^{1/2}}. \quad (1)$$

Here,  $ka^2$  is defined as the diffraction length,  $k$  is the wave number, and  $a$  is the radius of the beam profile. In Refs. [33,34], the critical power ( $P_{\text{cr}}$ ) was derived by measuring the focal shift of a single filament in air. In Fig. 2, the power that we used was beyond 22 times that of the critical power in water ( $P_{\text{cr}} = 4.2 \text{ MW}$ )<sup>[8,10]</sup>, which corresponded to  $\sim 0.25 \mu\text{J}$  of pulse energy according to the laser parameters used in our experiments. When the input peak power ( $P$ ) is far above the critical power ( $P_{\text{cr}}$ ) for self-focusing, the modulational instability breaks up the beam into a large number ( $N \approx P/P_{\text{cr}}$ ) of filaments<sup>[2,35–37]</sup>. In this sense, for both doped water and pure water, the plasma channel in Figs. 2(a), 2(c), and 2(e) consisted of multiple filaments. During our experiment, the imaging of filaments in water was able to be identified

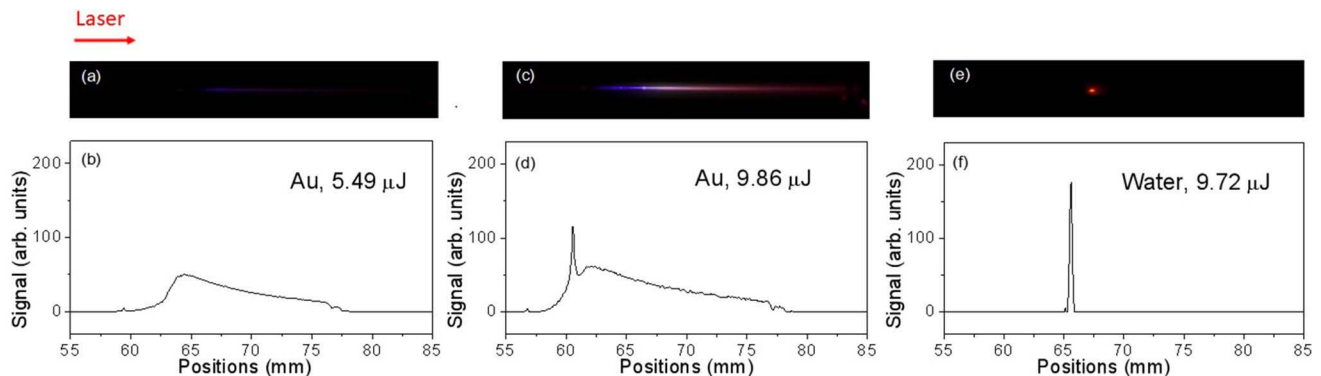


Fig. 2. Top views of light channel (top row) and the corresponding longitudinal white light intensity distribution in gold-nanoparticle-doped water (bottom row) with input pulse energy of (a), (b) 5.49  $\mu\text{J}$  and (c), (d) 9.86  $\mu\text{J}$  and in pure water with pulse energy of (e), (f) 9.72  $\mu\text{J}$ .

with input pulse energy beyond 1.1  $\mu\text{J}$ . For lower energy, the light channel became flickering dots (random filament distribution).

In liquids, filaments create high temperature zones, which further lead to convection and bubble generation<sup>[21–23]</sup>. Because of that, for input power around the critical power, a single filament is created and randomly distributed. The focal shift is not uniform as time changes. That means that the critical power cannot be retrieved by measuring the focal shift of a single filament<sup>[33,34]</sup>. However, with the increase of the laser power, multiple filaments are generated in a small scale, which provide a reservoir containing higher energy<sup>[38,39]</sup>. It finally stabilizes the onset of multiple filaments. The length of each child filament is normally tens to hundreds of microns in pure water<sup>[18]</sup>. In the case that the input power is ten times larger than the critical power, at the laser cross section, multiple child filaments unite and increase the diameter of filaments<sup>[38]</sup>. At the longitudinal axis, they also connect and lengthen the plasma channel. Besides, in the focusing geometry of a high energy laser pulse, in the direction of laser propagation, the number of child filaments gradually increases from the tip of multifilaments until their most intense party. Thus, we assume that there is only one quite short (several microns) single filament that was created at the tip of the filaments. In this sense, the critical power is evaluated by measuring the shift of the tip (starting position) of the multiple filaments.

We substituted the measured shifts into Eq. (1) in order to retrieve the critical power ( $P_{\text{cr}}$ ). Then, the nonlinear refractive index ( $n_2$ ) was derived according to the relation of  $P_{\text{cr}} = 3.77\lambda^2/8\pi n_0 n_2$ , with  $n_0$  and  $n_2$  being the linear index of refraction and second-order nonlinear index coefficient. In Table 1, when taking  $n_0 = 1.33$  in water, the nonlinear refractive index in water was measured to be  $3.04 \times 10^{-16} \text{ cm}^2/\text{W}$ . The typical value of nonlinear refractive index is  $2 \times 10^{-16} \text{ cm}^2/\text{W}$  in water<sup>[3]</sup>. The measured nonlinear refractive index in gold-nanoparticle-doped water is more than 6 times larger than the typical value of the nonlinear refractive index in pure water. Figure 3 shows the changes of the starting position of multifilaments in terms of  $P/P_{\text{cr}}$ . We combine Eq. (1) with the lens transformation formula in order to fit the experimental curve. In Fig. 3, the calculated onset shifts of

**Table 1.** Measured Critical Power ( $P_{\text{cr}}$ ) and Nonlinear Refractive Index ( $n_2$ ) in Gold-nanoparticle-doped Water and Pure Water Under Different Input Pulse Energy

	Pulse Energy ( $\mu\text{J}$ )	Critical Power $P_{\text{cr}}$ (MW)	Nonlinear Refractive Index $n_2$ ( $\text{cm}^2/\text{W}$ )
Doped water	5.49	0.48	$15.0 \times 10^{-16}$
Doped water	9.86	0.53	$13.6 \times 10^{-16}$
Pure water	9.72	2.35	$3.04 \times 10^{-16}$

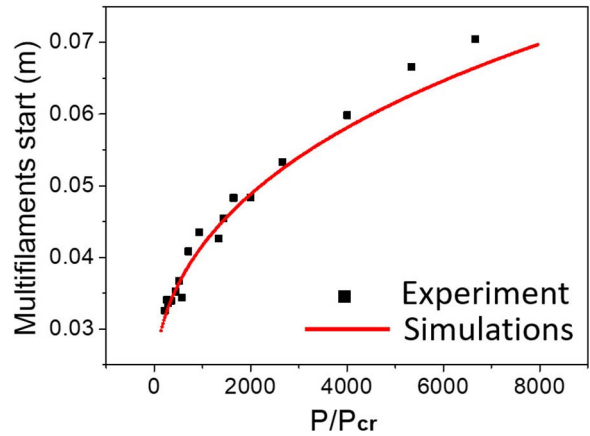


Fig. 3. Starting position of multifilaments as a function of  $P/P_{\text{cr}}$  (input power divided by critical power) in gold-nanoparticle-doped water. Solid squares, experimental results; red line, simulations. We take  $P_{\text{cr}} = 0.5 \text{ MW}$  for the critical power of self-focusing in doped water by considering the results in Table 1.

filaments are in good agreement with the directly measured starting position changes of filaments. This not only verifies the accuracy of our measurement, but also provides an alternative approach for estimating the nonlinear refractive index in liquids, e.g., in water and doped water, through measuring the shifts of the starting position of multiple filaments. The advantage is that the location of multiple filaments is much easier to identify than that of a single filament in liquids.

In order to provide a more complete physical picture of filamentation in gold-nanoparticle-doped water, the output spectra at the exit of the cuvette were measured by using the experimental setup in Fig. 1. The results are shown in Fig. 4. It is known that filamentation-induced frequency variation can be explained by<sup>[8]</sup>

$$\Delta\omega(t) \approx -\frac{\omega_0 z n_2}{c} \frac{\partial I(t)}{\partial t} + \frac{2\pi e^2 N_0 z}{c m_e \omega_0} I^m(t), \quad (2)$$

where  $z$  is the propagation distance,  $c$  is the speed of light in vacuum,  $m$  is the effective nonlinear order of excitation,  $N_0$  is the number of initially present neutral particles in the focal volume,  $\omega_0$  is the central frequency of the laser pulse, and  $e$  and  $m_e$  are the electronic charge and mass, respectively. Equation (2) represents the frequency shift due to the time-dependent variation of the nonlinear refractive index. For low average input energy, the frequency modulation is dominated by self-phase modulation  $-\frac{\omega_0 z n_2}{c} \frac{\partial I(t)}{\partial t}$ , which basically creates a symmetric spectral broadening of the output spectra<sup>[40]</sup>. Accordingly, in Fig. 4(a), for both doped water and pure water, the spectra broaden around  $\lambda_0 = 800 \text{ nm}$  with peaks rising symmetrically about the fundamental wavelength (see the green, dark yellow, red solid curves). Meanwhile, in Fig. 4(a), the output spectra around  $\lambda_0 = 800 \text{ nm}$  measured after the filament in doped water are broader than those in pure water. Stronger spectral

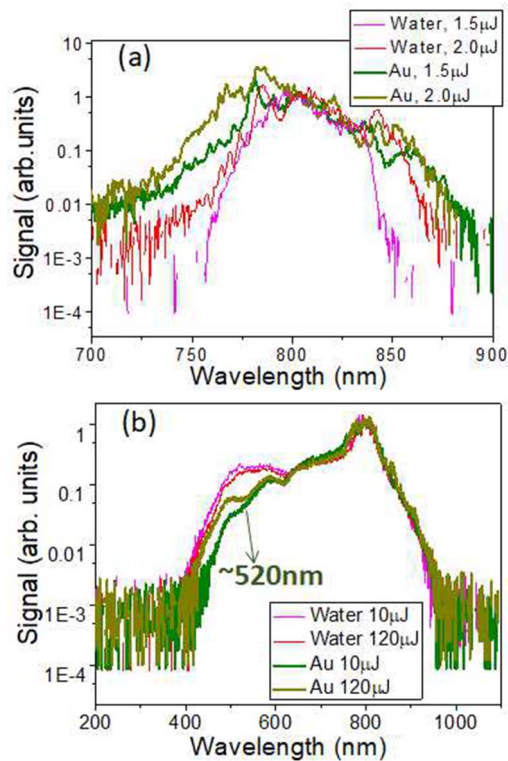


Fig. 4. Spectra obtained for the propagation of the laser pulse in gold-nanoparticle-doped water (green and dark yellow solid curves) as compared with those in pure water (pink and red solid curves) under (a) low and (b) high average input energy. The spectra are normalized to the intensity of the signal at 800 nm.

modulation in doped water indicates a larger nonlinear refractive index, which is in good accordance with the results in Table 1. While for high average input energy, the frequency modulation is dominated by the plasma generation. It gives rise to the blue frequency shift of the output spectra, which are shown in Fig. 4(b). In Fig. 4(b), the white light component around 520 nm was absorbed through resonant absorption of 12 nm gold nanoparticles in doped water. Generally speaking, the generated white light around 520 nm in doped water excites the electrons of gold nanoparticles through SPRs, which finally leads to enhanced nonlinearity.

In conclusion, we have experimentally investigated filamentation in gold-nanoparticle-doped water. The generated white light spectrum in gold-nanoparticle-doped water overlaps SPRs of gold nanoparticles. As a result, the nonlinear refractive index in water is largely increased. It indicates that filamentation can be initiated with lower input power.

Nowadays, high field chemical reactions have already revealed detailed physical pictures for molecular science and demonstrated their applications in precision measuring technology and nanomaterial fabrication. Laser filamentation in metal-nanoparticle-doped liquids could be an alternative approach for triggering chemical reactions in solutions. The reasons are as follows. (i) The resulted larger nonlinearity is preferred by high-order processes.

(ii) The strong imaginary part of the resonant refractive index indicates resonant absorption, which increases temperature locally in water. High temperature zones cause shock wave generation and further lead to stronger water convection (laser-induced stirring), which motivates more molecules to join the reactions. (iii) Most metal nanoparticles, e.g., gold nanoparticles, are promising catalysts for chemical reactions. In this sense, it provides a perfect scheme to investigate the filamentation in metal-nanoparticle-doped liquids.

This work was supported by the National Key Research and Development Program of China (No. 2018YFB0504400), the National Natural Science Foundation of China (Nos. 61505106 and 11504237), the Innovation Program of Shanghai Municipal Education Commission (No. 201701070007E00007), and the Shanghai Chenguang Project (No. 15CG51).

## References

1. A. Couairon and A. Mysyrowicz, *Phys. Rep.* **441**, 47 (2007).
2. L. Bergé, S. Skupin, R. Nuter, J. Kasparian, and J. P. Wolf, *Rep. Prog. Phys.* **70**, 1633 (2007).
3. A. Brodeur and S. L. Chin, *Phys. Rev. Lett.* **80**, 4406 (1998).
4. A. Dubietis, G. Tamošauskas, I. Diomin, and A. Varanavičius, *Opt. Lett.* **28**, 1269 (2003).
5. J. S. Liu, H. Schroeder, S. L. Chin, R. X. Li, W. Yu, and Z. Xu, *Phys. Rev. A* **72**, 053817 (2005).
6. Z. Liu, Y. Zhang, J. Ding, S. Sun, and B. Hu, *Chin. Opt. Lett.* **15**, 021401 (2017).
7. W. Liu, S. L. Chin, O. Kosareva, I. Golubtsov, and V. Kandidov, *Opt. Commun.* **225**, 193 (2003).
8. W. Liu, O. Kosareva, I. Golubtsov, A. Iwasaki, A. Becker, V. Kandidov, and S. L. Chin, *Appl. Phys. B* **76**, 215 (2003).
9. M. Kolesik, E. Wright, and J. Moloney, *Phys. Rev. Lett.* **92**, 107 (2004).
10. W. Liu, S. Petit, A. Becker, N. Akozbek, C. Bowden, and S. L. Chin, *Opt. Commun.* **202**, 189 (2002).
11. L. Wang, Y. Fan, Z. Yan, H. Wang, and Z. Wang, *Opt. Lett.* **35**, 2925 (2010).
12. H. H. Fan, Y. J. He, J. W. Dong, B. C. Chen, H. Z. Wang, Y. P. Tian, and M. F. Reid, *Appl. Phys. Lett.* **96**, 021109 (2010).
13. S. Chekalin, A. Dokukina, A. Dormidonov, V. Kompanets, E. Smetanina, and V. Kandidov, *J. Phys. B: At. Mol. Opt. Phys.* **48**, 094008 (2015).
14. Y. Geints, A. Zemlyanov, A. Kabanov, G. Matvienko, and A. Stepanov, *Quantum Electron.* **43**, 350 (2013).
15. H. Fan, K. Wu, H. Wang, Y. Tian, G. Law, K. Wong, and W. Wong, *Chem. Phys. Lett.* **449**, 77 (2007).
16. Q. Cui, J. Yao, J. Ni, and S. Zhang, *J. Mod. Opt.* **59**, 1569 (2012).
17. V. Jukna, V. Jarnac, C. Milián, Y. Brelet, J. Carbonnel, Y. André, R. Guillermin, J. Sessarego, D. Fattaccioli, A. Mysyrowicz, A. Couairon, and A. Houard, in *Conference on Lasers and Electro-Optics* (2016), paper JW2A.38.
18. F. Potemkin, E. Mareev, A. Podshivalov, and V. Gordienko, *New J. Phys.* **17**, 053010 (2015).
19. F. Potemkin and E. Mareev, *Laser Phys. Lett.* **12**, 015405 (2015).
20. J. A. Dharmadhikari, G. Steinmeyer, G. Gopakumar, D. Mathur, and A. K. Dharmadhikari, *Opt. Lett.* **41**, 3475 (2016).
21. J. Ye, G. Chang, T. Norris, C. Tse, M. Zohdy, K. Hollman, M. Donnell, and J. Baker, *Opt. Lett.* **29**, 2136 (2004).

22. D. Faccio, G. Tamošauskas, E. Rubino, J. Darginavičius, D. G. Papazoglou, S. Tzortzakis, A. Couairon, and A. Dubietis, *Phys. Rev. E* **86**, 036304 (2012).
23. F. Liu, S. Yuan, Z. Zuo, W. Li, L. Ding, and H. Zeng, *Opt. Express* **24**, 13258 (2016).
24. V. Amendola and M. Meneghetti, *Phys. Chem. Chem. Phys.* **11**, 3805 (2009).
25. L. Caspani, R. Kaipurath, M. Clerici, M. Ferrera, T. Roger, J. Kim, N. Kinsey, M. Pietrzyk, A. Falco, V. Shalaev, A. Boltasseva, and D. Faccio, *Phys. Rev. Lett.* **116**, 233901 (2016).
26. M. Stockman, D. Bergman, C. Anceau, S. Brasselet, and J. Zyss, *Phys. Rev. Lett.* **92**, 057402 (2004).
27. S. Kim, J. Jin, Y. Kim, I. Park, Y. Kim, and S. Kim, *Nature* **453**, 757 (2008).
28. S. Lal, S. Link, and N. Halas, *Nat. Photon.* **1**, 641 (2007).
29. L. Novotny and N. van Hulst, *Nat. Photon.* **5**, 83 (2011).
30. C. Wang, Y. Fu, Z. Zhou, Y. Cheng, and Z. Xu, *Appl. Phys. Lett.* **90**, 181119 (2007).
31. R. Driben, A. Husakou, and J. Herrmann, *Opt. Lett.* **34**, 2132 (2009).
32. P. Vasa, M. Singh, R. Bernard, A. Dharmadhikari, J. Dharmadhikari, and D. Mathur, *Appl. Phys. Lett.* **103**, 111109 (2013).
33. W. Liu and S. Chin, *Opt. Express* **13**, 5750 (2005).
34. H. Li, W. Chu, H. Zang, H. Xu, Y. Cheng, and S. L. Chin, *Opt. Express* **24**, 3424 (2016).
35. F. Vidal and T. Johnston, *Phys. Rev. Lett.* **77**, 1282 (1996).
36. G. Fibich, S. Eisenmann, B. Ilan, Y. Erlich, M. Fraenkel, Z. Henis, A. Gaeta, and A. Zigler, *Opt. Express* **13**, 5897 (2005).
37. G. Fibich and B. Ilan, *Opt. Lett.* **26**, 840 (2001).
38. T. Wang, Y. Chen, C. Marceau, F. Théberge, M. Châteauneuf, J. Dubois, and S. Chin, *Appl. Phys. Lett.* **95**, 131108 (2009).
39. S. Hosseini, Q. Luo, B. Ferland, W. Liu, S. Chin, O. Kosareva, N. Panov, N. Aközbek, and V. Kandidov, *Phys. Rev. A* **70**, 033802 (2004).
40. R. W. Boyd, *Nonlinear Optics*, 2nd ed. (Academic, 2003).